

The Shift of Breakdown Voltage for Silicon Membrane Strip Detectors Resulting from Surface Avalanche

W. Peng,^{1, a)} I. Sabri Alirezaei,² N. André,² X. Zeng,² M. Bouterfa,² B. Wang,¹ Y. Zeng,¹ and D. Flandre²

¹⁾Key Laboratory for Micro/Nano Optoelectronic Devices of Ministry of Education, and the Hunan Provincial Key Laboratory of Low-Dimensional Structural Physics and Devices, School of Physics and Electronics, Hunan University, Changsha 410082, China.

²⁾Institute of Information and Communication Technologies, Electronics and Applied Mathematics (ICTEAM), Université catholique de Louvain, 1348 Ottignies-Louvain-la-Neuve, Belgium

(Dated: 16 May 2021)

Silicon membrane strip photodetectors are fabricated based on thin silicon-on-insulator (SOI) wafers. The thin SOI wafer is realized by exploiting a thinning process on back-side. Such detectors can be implemented in proton-beam position detection because its ultra-thin membrane substrate can reduce beam scattering and offer the considerable advantages of a higher radiation hardness. A p-spray implantation process is typically performed at the silicon surface between the n⁺-strips in order to insulate them, without requiring an extra photolithographic mask. In this paper, the sources of leakage current in the detector are firstly studied by considering both activation energy and simulation analysis in Silvaco TCAD. While the device is operating below avalanche breakdown voltage, the Shockley-Read-Hall (SRH) process and trap-assisted-tunneling (TAT) process are dominantly contributing in leakage current. The dominant breakdown voltage is attributed to the premature breakdown in the junction of p-spray/n⁺-region. The shift of this breakdown voltage under repeated avalanche processes is analyzed in-depth by both experiments and simulations, as a function of temperature and electrical stress conditions, which are introducing an important reliability problem. The electrical stress can be attributed to an increase of fixed charge density at the Si/SiO₂ interface. The breakdown voltage finally increases by 4 V after successive avalanche breakdowns as function of the applied excess bias voltage beyond breakdown voltage.

I. INTRODUCTION

Silicon strip detectors are widely used for vertexing and tracking of charged particles in nuclear and particle physics experiments¹. Strip photodetectors integrated with a scintillator have also been implemented in Gamma-ray position detectors^{2,3}. In this case, incident Gamma-ray activates the scintillator and light is generated⁴. The peak wavelength of scintillation light can be selected in visible spectral range of relevance for Si, but to detect the low generated intensity, the silicon strip detectors have to be highly sensitive. Other position sensitive detectors (PSDs) have been widely used in diverse applications including optical engineering, aerospace, and military fields based on the lateral photo effect⁵⁻⁷. A strip detector fabricated on a silicon membrane can be implemented as a proton-beam detector which can monitor the proton-beam in real time in order to know the actual dose deposited into the targets. In addition to a reduced beam scattering, ultra-thin detectors offer a higher radiation hardness which leads to an improved detector life time and a much better collection efficiency^{8,9}.

In this paper, we extend the investigation of a silicon membrane strip detector based on silicon-on-insulator (SOI) layer, fabricated by a simple silicon thinning process of the bulk wafer, initially designed for a proton-beam application as discussed above. The ultra-thin silicon membrane provides a possibility of either two-dimensional or even three-dimensional detection systems by stacking several thin layers that can all be traversed by the proton beam.

However, parasitic positive charge build-up in the field-oxide insulating layer between the strips, related to process defects during fabrication or radiation degradation under operation, causes electrons to accumulate at the Si/SiO₂ surface, which can lead to increased leakage current or even a short circuit between the strips^{10,11}. A p-spray technology, which does not require an extra mask and consists in a uniform p-type blanket implant, is performed on the silicon surface to insulate each strip. The p-spray disadvantage can be higher strip capacitance and reduced breakdown voltage as discussed below.

In order to achieve high responsivity, the strip detector is often operated under high reverse bias to enlarge the depletion region and hence carrier collection region. However, when avalanche breakdown happens, the huge current flow density can lead to the breakdown shift of the detector by localized Joule heating at high temperature, high density of charge accumulation at the interfaces etc. The leakage current and breakdown voltage (V_{br}), which can be significantly changed by process or huge avalanche current flow, are amongst the most important parameters to characterize the device reliability. The physical mechanism of V_{br} shift has been studied, for example, in SiC diodes¹², power MOSFETs¹³ and GaN HEMTs¹⁴. However, no research works focused on the V_{br} shift caused by avalanche breakdown in silicon strip detectors.

In this paper, the components of leakage current, the source of the breakdown shift in the membrane strip detectors and their physical mechanisms are analyzed and explained by experiments and simulations.

^{a)}Electronic mail: pengwei@hnu.edu.cn

This is the author's peer reviewed, accepted manuscript. However, the online version of record will be different from this version once it has been copyedited and typeset.
PLEASE CITE THIS ARTICLE AS DOI: 10.1063/1.50049490

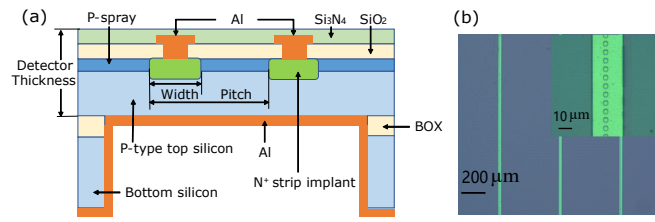


FIG. 1. Structure of the strip detector. (a) Cross-section schematic view. (b) Plane-section view taken by optical microscope, in which the inserted figure shows an enlarged strip electrode, and the small squares are the contact holes.

II. DEVICE STRUCTURE AND EXPERIMENTAL DETAILS

Fig.1(a) shows a schematic cross-section view of a pair of strips on SOI membrane. Considering the trade-off between spatial detecting resolution and the requirements for the number of readout channels, the pitch length is designed as 500 μm in a proton-beam detector. The length and the width of the N^+ strips are 1.5 cm and 30 μm respectively. The strip doping depth is about 1 μm and the silicon membrane thickness is 20 μm .

The detectors were fabricated on p-type double-side polished blank thick SOI wafers with a bottom silicon thickness of 400 μm , a buried oxide (BOX) of 500 nm and a top silicon thickness of 20 μm . The top silicon layer acts as the ultra-thin membrane after etching the bottom silicon substrate below the detector. The substrate and SOI layer doping concentration was about 10^{15} to 10^{16} cm^{-3} .

The strip detectors were firstly fabricated on the frontside of the starting wafers. A wet-thermal oxide of 300 nm was grown as a hard mask for the backside thinning, and a wet-thermal oxide of 100 nm was grown as a protection layer on the frontside to reduce the silicon damages caused by the implantation. For N^+ strip implantation, arsenic with a 100 keV energy and a 10^{16} ions/ cm^2 dose was implanted to get a bit more than 10^{21} cm^{-3} arsenic doping concentration at the oxide/silicon interface. For P-spray implantation, the boron implantation energy was 13 keV and its dose was 1.7×10^{12} ions/ cm^2 , yielding a p-type of about 10^{17} cm^{-3} at the Si surface. The thickness of the P-spray layer is about 0.2 μm . For strip contact holes, a reactive ion etching (RIE) was performed with a CHF_3 plasma for 25 min at 60 W to etch the contact holes anisotropically. Strips were then metallized by depositing a 250 nm Al/Si (1%) layer to reduce spiking effect. In order to protect the device from its environment, a nitride passivation layer of 300 nm was deposited by plasma enhanced chemical vapor deposition (PECVD) over the whole frontside surface. The passivation layer was then dry etched by SF_6 to open the contact pads for electrical connections with the device.

Secondly, the thinning step was performed. Backside photolithography is aligned for thinning area patterning, and then we etched the backside oxide, which acted as a hard mask against TMAH, over the thinning area with a BHF solution in 6 min. The frontside was then protected via the Protek re-

sist. Afterwards, the wafers were placed in a 5% TMAH bath at 95 $^\circ\text{C}$ for about 10 hours. For the BOX release, a RIE with a CHF_3 plasma was performed for 25 min. Finally, the back metallization was a 250 nm thick aluminum layer which was then silicided through an annealing at 432 $^\circ\text{C}$ for 30 min. As shown in Fig.1(b), the fabricated strip detector is of high quality from the plane section view taken by an optical microscope. The full detector features 80 parallel strips over a membrane area of 4.2×1.7 cm^2 . The present study is next focused on single strips measured individually while grounding the neighbor ones.

III. CHARACTERIZATION RESULTS

A. Leakage current

In terms of physical principles, there can be two main sources for the leakage current in the strip detector, i.e., the diffusion current and Shockley-Read-Hall (SRH) process related current¹⁵. The diffusion current is the intrinsic leakage current which comes from the flow of thermally-generated electrons and holes through the junction. The SRH related component is the generation of minority carriers in the depletion region, governed by the SRH process. The latter is generally dominant in Si diodes at temperatures below and moderately above 400 K.

Concerning the flows of carriers, the leakage current is formed by surface leakage flow and bulk leakage flow. The surface leakage current originates from the generation of minority carriers at the Si surface and along the perimeters of the strips due to the high interface-state density at Si/SiO₂ interfaces, which is governed by a Shockley-Read-Hall (SRH) process. The bulk leakage current can also be attributed to both a Shockley-Read-Hall (SRH) process in the vertical depletion region below the strips and to the diffusion process across it. The trap-assisted-tunneling (TAT) process, occurring along with the SRH process under strong electric field, is considered as an enhancement to the SRH-related minority carrier generation for both the surface leakage current and bulk leakage current¹⁵, notably below avalanche breakdown voltage.

Dark I-V curves of single strips under a temperature from 30 $^\circ\text{C}$ to 80 $^\circ\text{C}$ were measured on a SuSS PM8PS probe station combined with the Agilent B1500 Semiconductor Device Analyzer. The activation energy (E_a) can be extracted from the slope of the linear relationship between $\ln(I_{\text{dark}})$ and $1/kT$. If the value of E_a is equal to the Si bandgap, the diffusion current density is dominant in leakage current. Besides, if the value of E_a is equal to half of the Si bandgap, the SRH process related current density is dominant in leakage current. Under higher reverse bias voltage (i.e. close to breakdown voltage), the value of E_a can become less than half of the Si bandgap due to the contribution of temperature dependent TAT enhancement factor^{15,16}. In this case, the activation energy of the SRH related leakage current density is contributed by the temperature dependent TAT enhancement factor.

For the extraction of activation energies (E_a), dark currents

This is the author's peer reviewed, accepted manuscript. However, the online version of record will be different from this version once it has been copyedited and typeset. PLEASE CITE THIS ARTICLE AS DOI: 10.1063/5.0049490

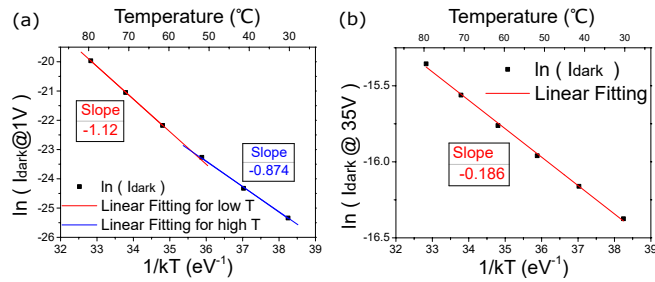


FIG. 2. Arrhenius plot of the dark current at fixed reverse voltage of (a) -1V and (b) -35V. For figure (a), the red line is the fitting of the experiment data for temperature higher than 60 °C, and the blue line is the fitting of the experiment data for temperature lower than 50 °C.

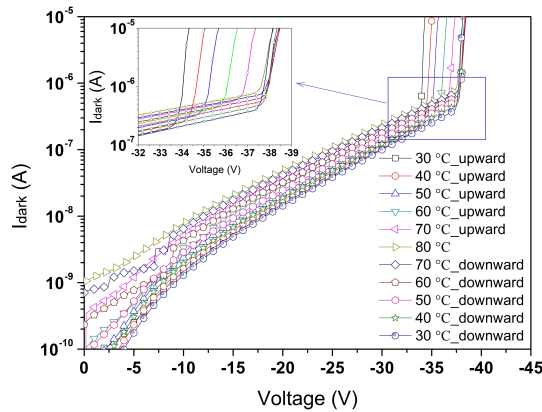


FIG. 3. Dark I-V curves for ramping up the temperature from 30 °C to 80 °C, and then ramping down to 30 °C, with 10 °C interval scale. The detectors underwent successive avalanche breakdowns with a current compliance at 1 mA in the measurements.

at a fixed bias voltage of -1 V and -35 V were investigated as a function of $1/kT$ (Arrhenius plot)¹⁶. As shown in Fig.2(a), when the device is biased at -1 V, the E_a above 60 °C is 1.12 eV equal to the Si bandgap. E_a decreases to 0.87 eV for the temperature range between 30 and 50 °C. This indicates that the dominant leakage current at low bias voltage originates from diffusion current especially when the temperature is above 60 °C, and the portion of SRH current density in the leakage current increases with decreasing temperature.

However, as shown in Fig.2(b), E_a at a high bias voltage of -35 V is about 0.19 eV. This value is below the half of the Si bandgap, which is attributed to the influence of TAT process occurring under a relatively strong electric field. Thus, the SRH related leakage current enhanced by TAT process is dominant at high bias voltage.

B. Shift of breakdown voltage

In order to study the variations of electrical parameters caused by temperature and avalanche breakdown current,

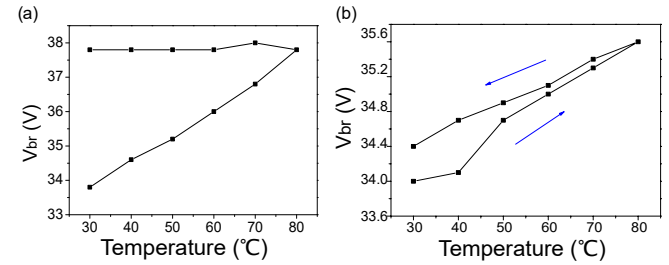


FIG. 4. Breakdown voltage shift with different temperature. (a) The compliance breakdown current is set at 1 mA which means the detector has undergone successive intense avalanche breakdowns. (b) The compliance breakdown current is set at 1 μ A which means the detector never experienced strong avalanche breakdown.

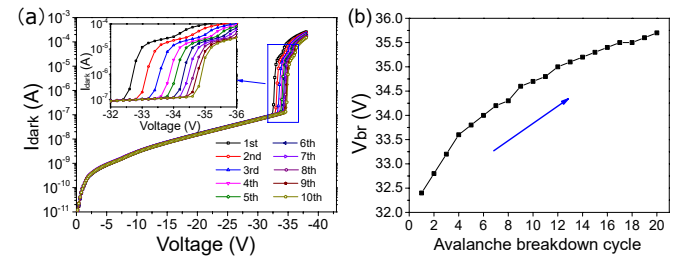


FIG. 5. Shift of breakdown voltage of the strip detector caused by repeated avalanche breakdown in room temperature. The compliance breakdown current is set at 1 mA. (a) I-V curves and (b) Shift of breakdown voltage with the increase of avalanche breakdown cycles.

dark I-V curves with different temperature under successive avalanche breakdowns were measured and are shown in Fig.3. The dark I-V curves were measured successively, ramping up the temperature from 30 °C to 80 °C, and then ramping down to 30 °C, with 10 °C interval and with a current compliance at 1 mA. The breakdown voltage increased by 4 V when the temperature was ramped from 30 to 80 °C, as shown in Fig.4(a). However, the value of breakdown voltage measured at 80 °C did not change when cooling down to 30 °C.

In order to understand the origin of the breakdown voltage shifting, we performed successive cycles of controlled avalanche processes under different conditions:

(a) The dark I-V curves of the strip detector were measured under reverse bias voltage up to breakdown voltage at different temperatures by setting the current compliance value at 1 μ A to avoid the degradation caused by huge current flow. As the hysteresis diagram shows in Fig.4(b), the breakdown voltage only increased from 34.0 V to 35.6 V with increasing temperature from 30 °C to 80 °C, and then went back to 34.4 V with the decreasing temperature. This increase of breakdown voltage (by 1.6 V) (Fig.4(b)) is much smaller than the increase of breakdown voltage caused by huge avalanche current, which is about 4 V (Fig.4(a)). However, the small difference of the breakdown voltages between initial values and cooled down values in the hysteresis curve of Fig.4(b) could be due to a lack of temperature control of detector itself or to a slight degradation of the detector.

(b) To further confirm the effect of avalanche breakdown

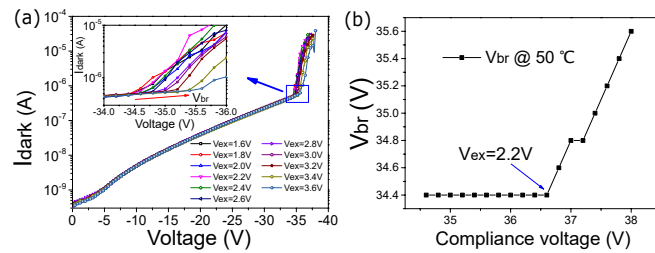


FIG. 6. Shift of breakdown voltage of the strip detector under increasing excess voltage (V_{ex}) at 50 °C. V_{ex} is the over-voltage applied in excess of the initial breakdown voltage which is 34.4 V in this measurement.

(a) I-V curves. (b) The shift of breakdown voltage after successively increasing compliance voltage for the I-V measurements.

on the shift of breakdown voltage, the dark I-V curves for the strip detector were measured at room temperature under multiple cycles of breakdown, as shown in Fig.5(a). The compliance breakdown current was set at 1 mA. As shown in Fig.5(b), after each avalanche process, the breakdown voltage increases continuously and irreversibly. The increased breakdown voltage was still measured and the same at the point of the last measurement after several months. This phenomenon is attributed to the several measurements under applied excess bias voltage beyond breakdown voltage (V_{ex}), resulting in a high current flow, an increase of TAT probability, and even a potential increase of fixed charge density in Si/SiO₂ interface. Therefore, the enhanced upward shift of breakdown voltage with temperature in Fig.4(a) originates from the V_{ex} as well as the decrease of the mean free path for carriers in silicon membrane caused by high temperature that we will discuss later.

(c) The shift of breakdown voltage is finally related to the stress-induced excess bias voltage. As shown in Fig.6(a), the I-V curves were measured with an increasing voltage compliance from 34.4 V to 38 V for a strip detector with an initial breakdown voltage of 34.4 V under the fixed temperature of 50 °C. The V_{ex} is the over-voltage applied in excess of the initial breakdown voltage. V_{ex} is here increases from 0 V to 3.6 V. As a result, the breakdown shift happens when the V_{ex} reaches 2.2 V, which can be seen in Fig.6(b). The corresponding avalanche current is 25 μ A. When the avalanche current is less than 25 μ A, the device undergoes light breakdown, which does not lead to significant V_{br} change of the device. However, when the avalanche current achieves 25 μ A, the shift of the V_{br} becomes stronger.

IV. DISCUSSION USING DEVICE SIMULATION

A. Simulation Setup

In order to understand the origin of leakage current and the physics leading to the V_{br} shift in depth, two-dimensional (2-D) numerical simulation for the device was performed in Silvaco Athena and Atlas. Because we mainly focus on the

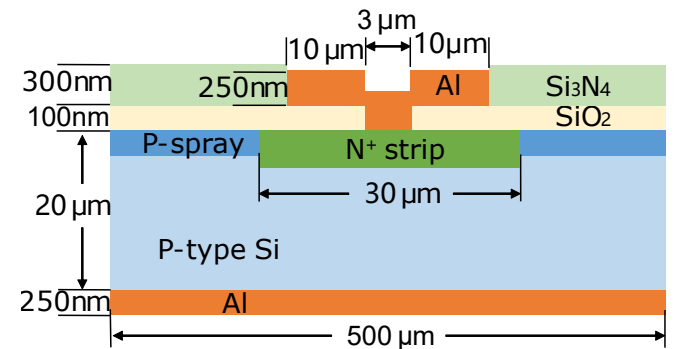


FIG. 7. Cross section of the strip detector implemented in 2-D Silvaco simulation.

TABLE I. Simulation Parameters for Implantation Process.

Implantation Process	Implantation Energy	Implantation Dose
N ⁺ Strip Implantation	100 keV	10 ¹⁶ ions/cm ²
P-spray Implantation	13 keV	1.7 x 10 ¹² ions/cm ²

physics of independent device, only a single strip centered between two other strips with a pitch of 500 μ m was simulated. First, we used Athena to simulate the device fabrication process. The setting of simulation parameters is consistent with the experimental fabrication process. The 2-D simulated device is illustrated in Fig.7, and the parameters for implantation are listed in Table I. After that, the simulation of electrical properties was performed in Atlas. It should be noted that the default parameters for physical models are used in our simulation and we didn't calibrate the full I-V curves, because we only focused on the physical phenomenon around breakdown.

B. Origin of leakage current

As for the leakage current, we have analyzed its composition from the physical principle by extracting the activation energies. In order to further understand the flow path of leakage current, the flow of leakage current is simulated, and Fig.8 shows the 2-D distribution of current density and current flow-lines. When the bias voltage is -1 V upon the temperature of 30 °C, the leakage current is mainly vertical bulk current. Moreover, the analysis of activation energy and the aforementioned simulated results show that the bulk current is consisting of diffusion current and SRH current originated from the vertical depletion region.

However, when the bias voltage is -35 V, as shown in Fig.8(c) and (d), the lateral surface current is dominantly contributing in the leakage current. This dominant surface current is the SRH related leakage current enhanced by TAT process, which is already presented by extracting the activation energy. In order to further verify this mechanism of current generation, we set up different simulation models in Atlas simulation. It can be seen from Fig.9, TAT related SRH mechanism

This is the author's peer reviewed, accepted manuscript. However, the online version of record will be different from this version once it has been copyedited and typeset.
PLEASE CITE THIS ARTICLE AS DOI: 10.1063/5.0049490

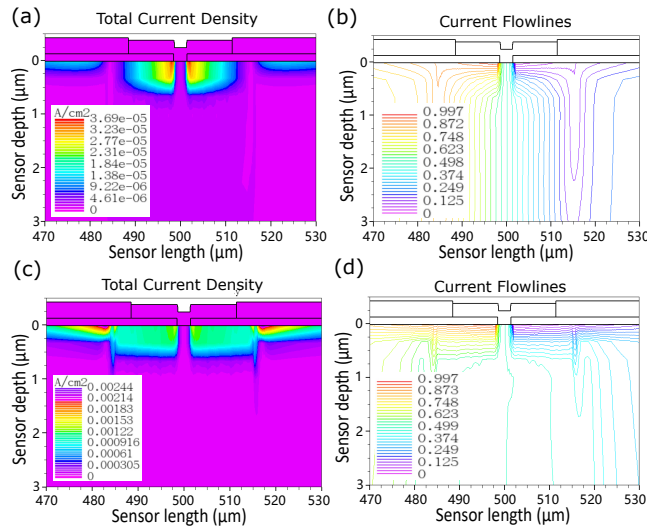


FIG. 8. Simulation results for one detector strip biased at low and high voltages, with the temperature set to 30 °C. (a) Leakage current density and (b) current flowlines for the detector biased at -1 V. (c) Leakage current density and (d) current flowlines for the detector biased at -35 V.

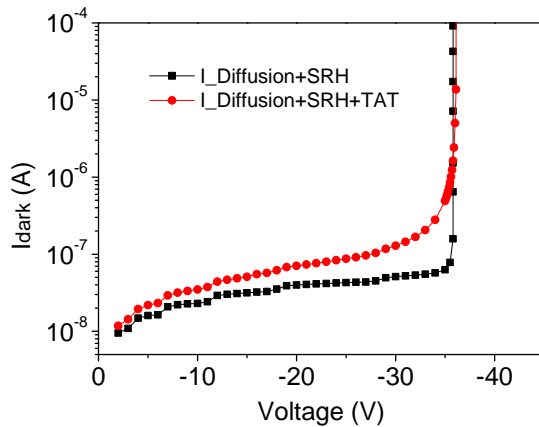


FIG. 9. Simulation results of the dark I-V curves with the different simulation models.

plays a dominant role when the device biased at high reverse voltage.

According to the higher doping level in the p-spray, the electric field at the n^+ /p-spray lateral junction is higher than at the bottom junction of n^+ /p-substrate, which causes a premature breakdown at the n^+ /p-spray/SiO₂ interface. As shown in Fig.8(c), at the surface of the n^+ /p-spray junctions, there is a region with extremely high current density at each side, where avalanche breakdown occurs first. In addition, as shown in Fig.5(a), a phenomenon of multiple breakdown steps can also be seen in dark I-V curves with a compliance current higher than 1 mA. In this case, the first breakdown happens at n^+ /p-spray junction, and the second at the vertical n^+ /p-substrate

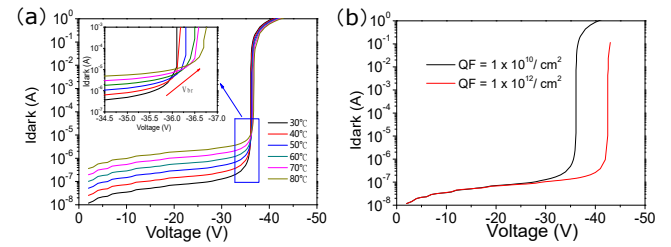


FIG. 10. Simulation results of the dark I-V curves (a) with different temperatures and a fixed positive charge density (QF) of $5 \times 10^{10}/\text{cm}^2$ at the Si/SiO₂ interface, and (b) with different QF at the Si/SiO₂ interface at room temperature.

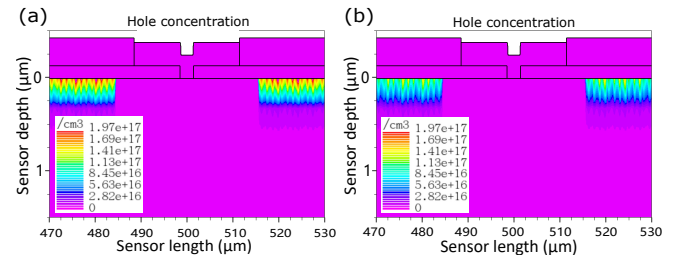


FIG. 11. The hole concentration distribution in the p-spray layer for QF = (a) $5 \times 10^{10}/\text{cm}^2$ and (b) $10^{12}/\text{cm}^2$.

junction below n-strips.

C. Shift of breakdown voltage

As shown in Fig.10(a), the simulation results show that the breakdown voltage increases with temperature, which is qualitatively confirming the experimental observations (Fig.4(b)). The mean free path in the depletion region for hot carriers decreases with increasing temperature of the crystal lattice, and the carriers must move through a greater potential until they acquire the necessary ionization energy for electron-hole pair generation. Thus, the breakdown voltage exhibits a positive temperature coefficient^{17,18}.

In order to study the breakdown shift caused by the interface states or dangling bonds, we simulated the I-V curves at room temperature with different densities of fixed positive charge (QF) at the Si/SiO₂ interface, as shown in Fig.10(b). The breakdown voltage increases with the increase of QF. The annealing post-process in forming gas is helpful to reduce the interface states or dangling bonds at the Si/SiO₂ interface. However, the interface states can be changed after several measurements due to the probability of an avalanche injection of hot carriers into the silicon oxide. Indeed, while the detector operates under breakdown voltage or even excess bias voltage, holes are accumulated at the Si/SiO₂ interface and injected into the silicon oxide layer, thereby increasing the concentration of fixed positive charges in the oxide layer¹⁹. As shown in Fig.11, the increased fixed positive charges in

the oxide layer repel the holes in the p-spray region, which is equivalent to reducing the p-doping concentration, thereby reducing the built-in electric field in n^+ /p-spray junction and increasing the breakdown voltage.

V. CONCLUSION

In this paper, we analyzed several reliability problems regarding the physics of leakage current and avalanche breakdown for a silicon membrane strip detector with a p-spray isolation layer, which can be applied in a proton-beam detector. The experimental activation energies and simulation results of the device under the reverse bias close to the avalanche breakdown indicate a superior contribution of the surface SRH related leakage current enhanced by TAT process. The shift of the breakdown voltage under successive avalanche processes was analyzed experimentally, a slight increase of V_{br} with temperature has been observed, according to theory, when the avalanche current is limited to a low compliance. Under strong avalanche process, the significant shift of V_{br} happens and V_{br} increases significantly and irreversibly. Simulations indicate that the first avalanche process is related to the breakdown of the surface n^+ /p-spray junction due to the high doping level in the p-spray. When the detector works under strong avalanche, hot holes are accumulated at the Si/SiO₂ interface and injected into the silicon oxide layer, thereby leading to the increase of V_{br} . This research will provide guidance for design and fabrication of silicon detectors with a p-spray layer.

ACKNOWLEDGMENTS

This work was supported in part by the Micro+ project funded by the European Regional Development Fund (ERDF) and Wallonia (Belgium), in part by the FRS-FNRS Convergence project (Belgium), in part by the National Natural Science Foundation of China under Grant 61705065, in part by the Hunan Provincial Natural Science Foundation of China No.2020JJ4214, and in part by CSC grants of China.

DATA AVAILABILITY STATEMENT

The data that support the findings of this study are available from the corresponding author upon reasonable request.

¹V. Chabaud, P. Collins, H. Dijkstra, J. J. Gomez Cadenas, R. Keranen, S. Masciocchi, and etc., “The delphi silicon strip microvertex detector with double sided readout,” Nucl. Instrum. Methods Phys. Res., Sect. A **368**, 314–332 (1996).

²D. H. Kah, J. B. Bae, H. J. Hyun, H. J. Kim, H. O. Kim, and H. Park, “Fabrication and performance test of a silicon photo-strip detector coupled with a crystal scintillator,” Nucl. Instrum. Methods Phys. Res., Sect. A **628**, 256–259 (2011).

³J. B. Bae, H. J. Hyun, D. H. Kah, H. J. Kim, H. O. Kim, and H. Park, “Development of a detector with two photo-strip sensors and a crystal scintillator between sensors,” in *2011 IEEE Nuclear Science Symposium Conference Record* (Valencia, Spain, 2011) pp. 1167–1170.

⁴B. D. Milbrath, A. J. Peurrung, M. Bliss, and W. J. Weber, “Radiation detector materials: An overview,” J. Mater. Res. **23**, 2561–2581 (2011).

⁵W. Wang, Z. Yan, J. Zhang, J. Lu, H. Qin, and Z. Ni, “High-performance position-sensitive detector based on graphenex2013;silicon heterojunction,” Optica **5**, 27–31 (2018).

⁶E. Fortunato, G. Lavareda, M. Vieira, and R. Martins, “Thin film position sensitive detector based on amorphous silicon p-i-n diode,” Rev. Sci. Instrum. **65**, 3784–3786 (1994).

⁷T. Zhao, Y. Peng, B. Li, R. He, K. Liang, R. Yang, and D. Han, “High-time resolved two-dimensional tetra-lateral position-sensitive silicon photomultiplier,” IEEE Electron Device Lett. **39**, 232–235 (2018).

⁸M. Bouterfa, G. Alexandre, E. C. Gil, and D. Flandre, “Charge collection mapping of a novel ultra-thin silicon strip detector for hadron therapy beam monitoring,” Nucl. Instrum. Methods Phys. Res., Sect. A **732**, 4 (2013).

⁹M. Bouterfa and D. Flandre, “Validation of a novel ultra-thin silicon strip detector for hadron therapy beam monitoring,” Journal of Circuits, Systems, and Computers **22** (2013).

¹⁰G. Pellegrini, C. Fleta, F. Campabadal, S. Díez, M. Lozano, J. M. Rafí, and M. Ullán, “Technology development of p-type microstrip detectors with radiation hard p-spray isolation,” Nucl. Instrum. Methods Phys. Res., Sect. A **566**, 360–365 (2006).

¹¹F. Celeste, L. Manuel, P. Giulio, C. Francesca, M. R. Joan, and U. Miguel, “P-spray implant optimization for the fabrication of n-in-p microstrip detectors,” Nucl. Instrum. Methods Phys. Res., Sect. A **573**, 4 (2006).

¹²S. Liu, C. Yang, W. Sun, Q. Qian, Y. Huang, X. Wu, M. Wu, Q. Yang, and L. Sun, “Repetitive-avalanche-induced electrical parameters shift for 4h-sic junction barrier schottky diode,” IEEE Trans. Electron Devices **62**, 5 (2015).

¹³D. Jabs, K. H. Bach, and J. Christoph, “Avalanche breakdown evolution under hot-carrier stress: a new microscopic simulation approach applied to a vertical power mosfet,” J. Comput. Electron. **17**, 8 (2018).

¹⁴B. Prasannanjanyulu, S. Mishra, and S. Karmalkar, “Analysis of the significant rise in breakdown voltage of gan hemts from near-threshold to deep off-state gate bias conditions,” IEEE Trans. Device Mater. Reliab. **19**, 8 (2019).

¹⁵H. Chen, P. Verheyen, P. D. Heyn, G. Lepage, J. D. Coster, S. Balakrishnan, P. Absil, G. Roelkens, and J. V. Campenhout, “Dark current analysis in high-speed germanium p-i-n waveguide photodetectors,” J. Appl. Phys. **119**, 213105 (2016).

¹⁶E. Engelmann, S. Vinogradov, E. Popova, F. Wiest, P. Iskra, W. Gebauer, S. Loebner, T. Ganka, C. Dietzinger, R. Fojt, and W. Hansch, “Extraction of activation energies from temperature dependence of dark currents of sipm,” J. Phys.: Conf. Ser. **675**, 042049 (2016).

¹⁷P. Mars, “Temperature dependence of avalanche breakdown voltage temperature dependence of avalanche breakdown voltage in p–n junctions,” Int. J. Electron. **32**, 23–37 (1972).

¹⁸C. Y. Chang, S. S. Chiu, and L. P. Hsu, “Temperature dependence of breakdown voltage in silicon abrupt p-n junctions,” IEEE Trans. Electron Devices **18**, 391–393 (1971).

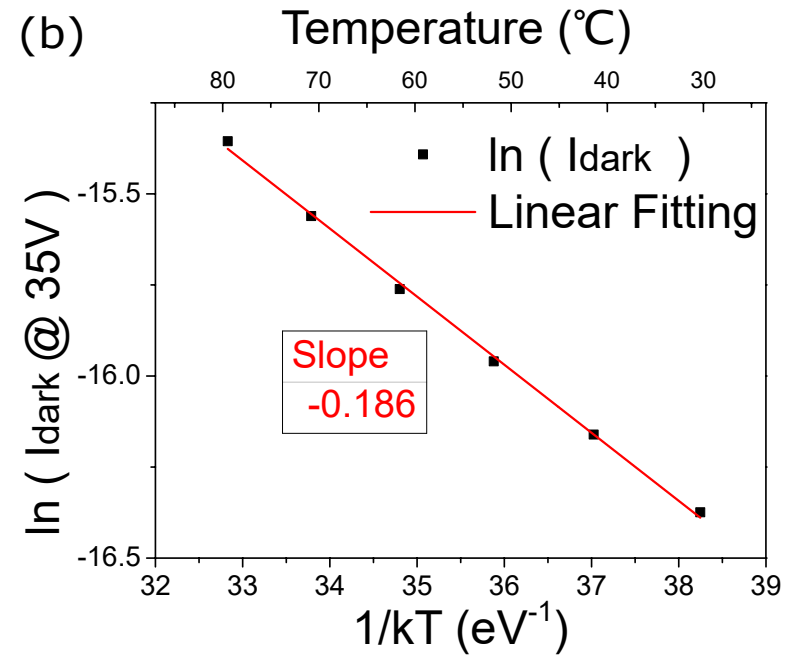
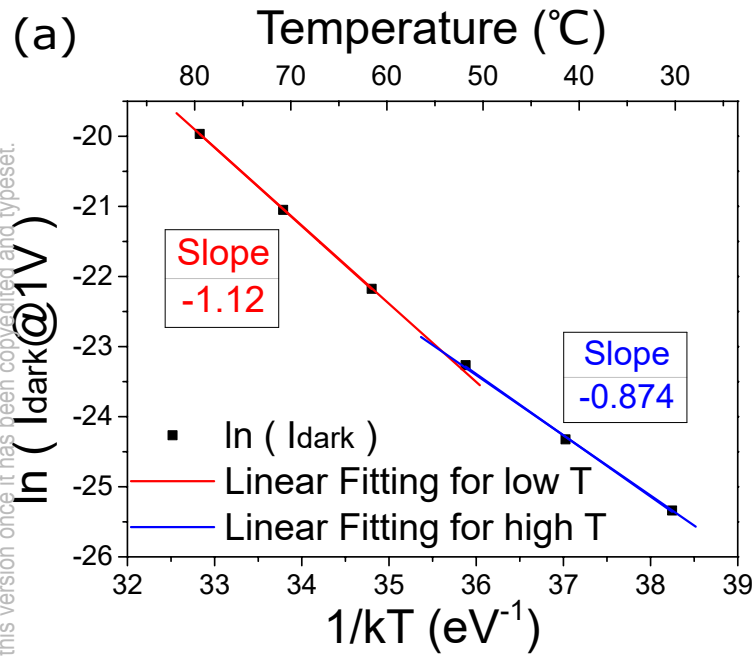
¹⁹C. M. Carbonaro, V. Fiorentini, and F. Bernardini, “Proof of the thermody-

This is the author's peer reviewed, accepted manuscript. However, the online version of record will be different from this version once it has been copyedited and typeset.

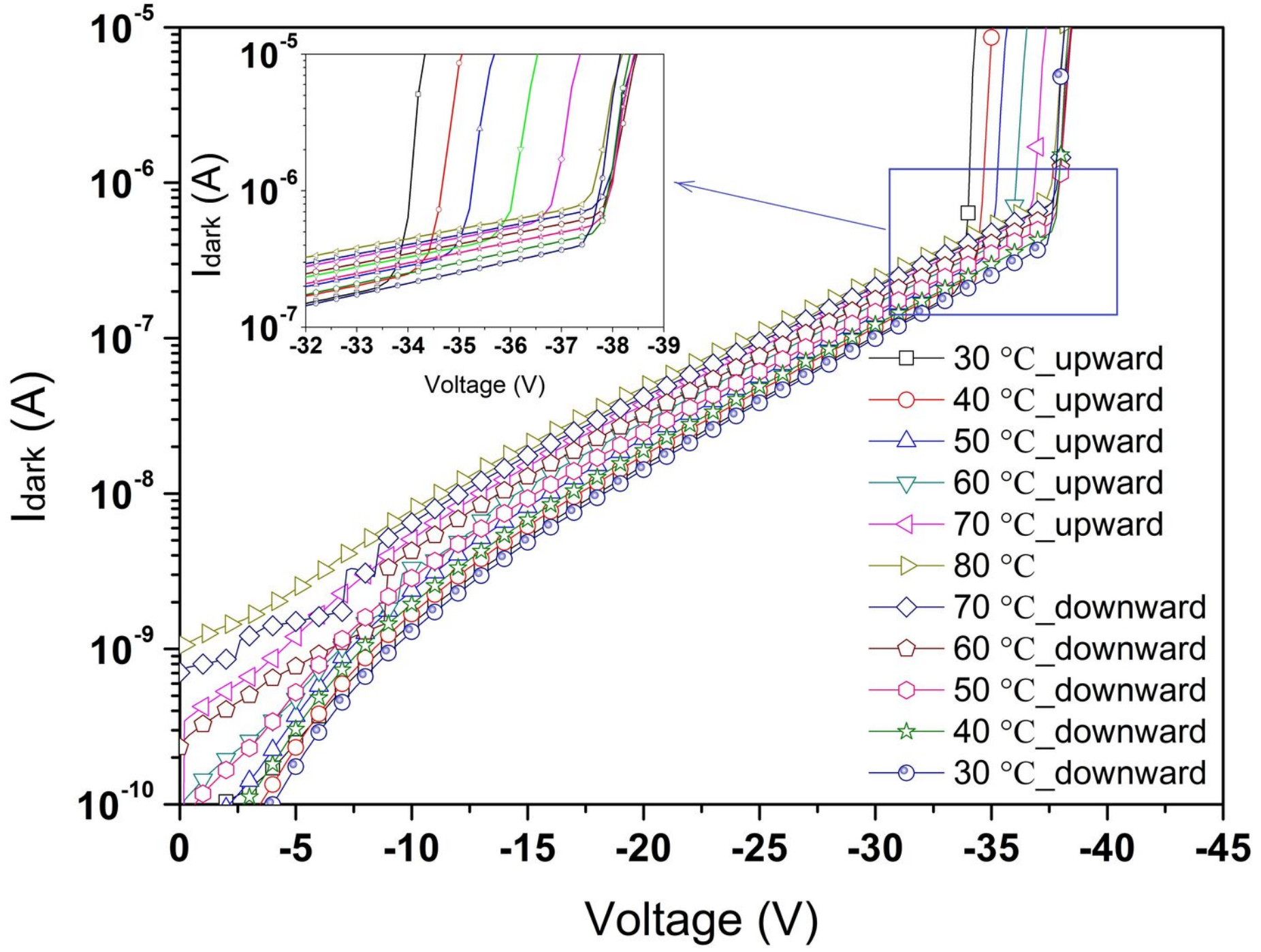
PLEASE CITE THIS ARTICLE AS DOI: 10.1063/5.0049490

namical stability of the e' center in SiO_2 ," Phys. Rev. Lett. **86**, 3064–3067 (2001).

This is the author's peer reviewed, accepted manuscript. However, the online version of record will be different from this version once it has been copyedited and typeset.
PLEASE CITE THIS ARTICLE AS DOI: 10.1063/5.0049490

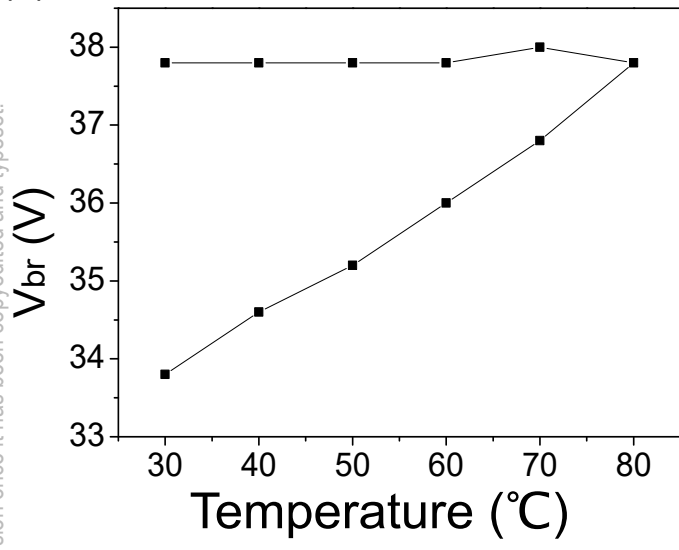


This is the author's peer reviewed, accepted manuscript. However, the online version of record will be different from this version once it has been copyedited and typeset.
PLEASE CITE THIS ARTICLE AS DOI: 10.1063/5.0049490

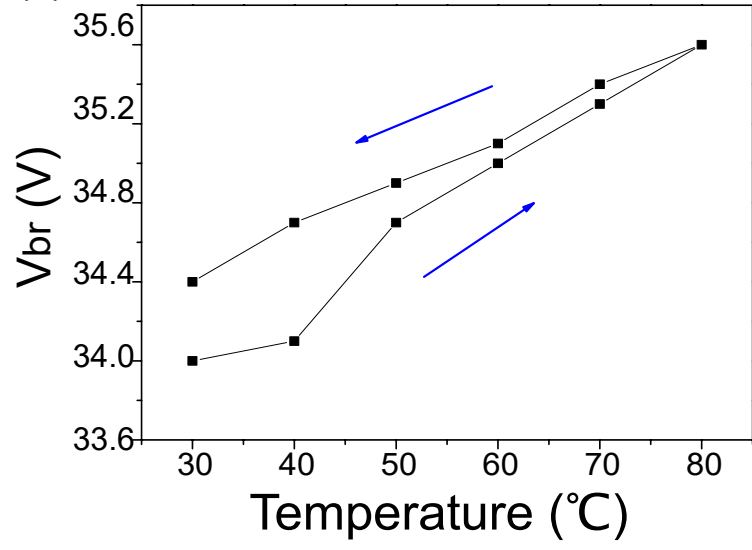


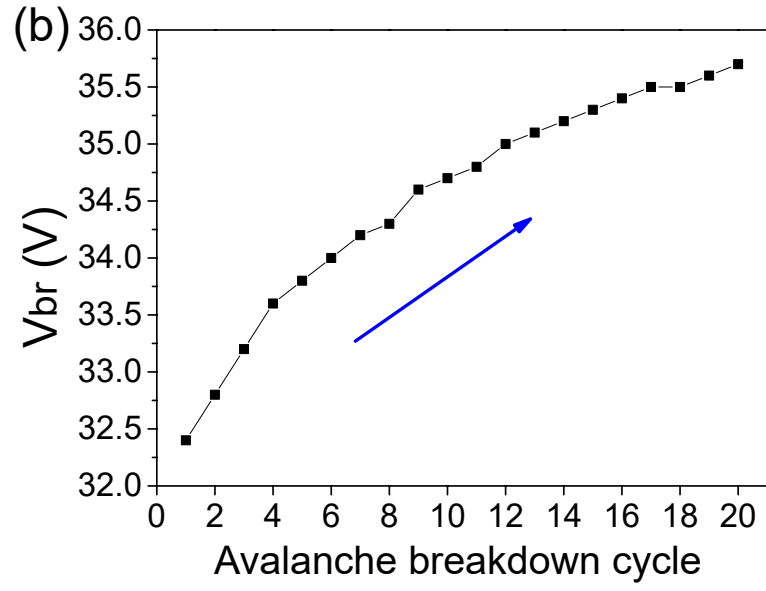
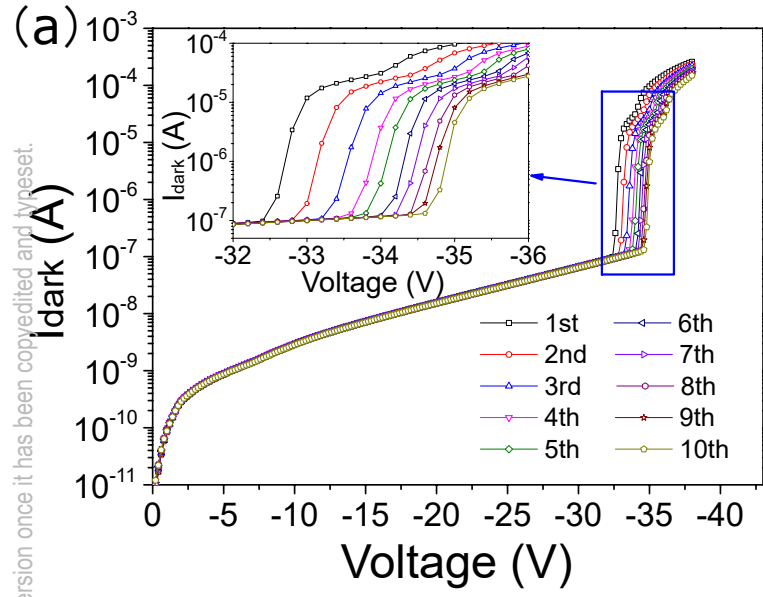
This is the author's peer reviewed, accepted manuscript. However, the online version of record will be different from this version once it has been copyedited and typeset.
PLEASE CITE THIS ARTICLE AS DOI: 10.1063/5.0049490

(a)



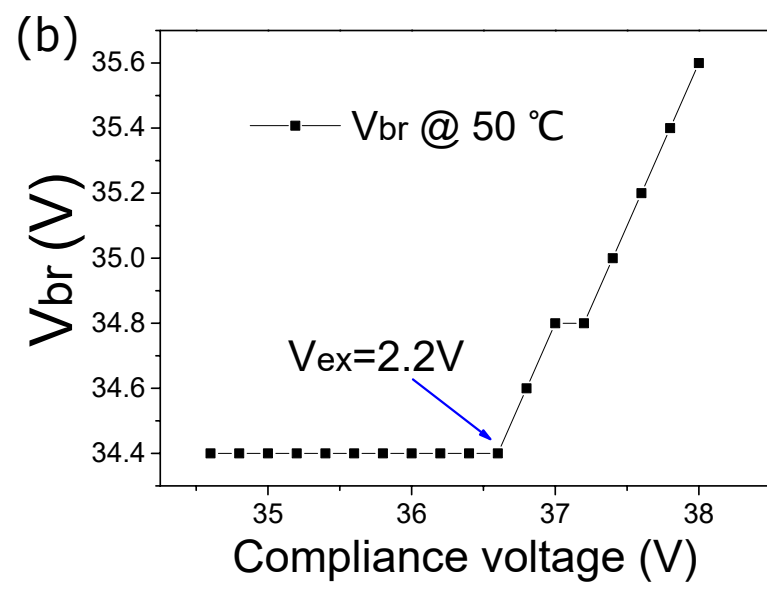
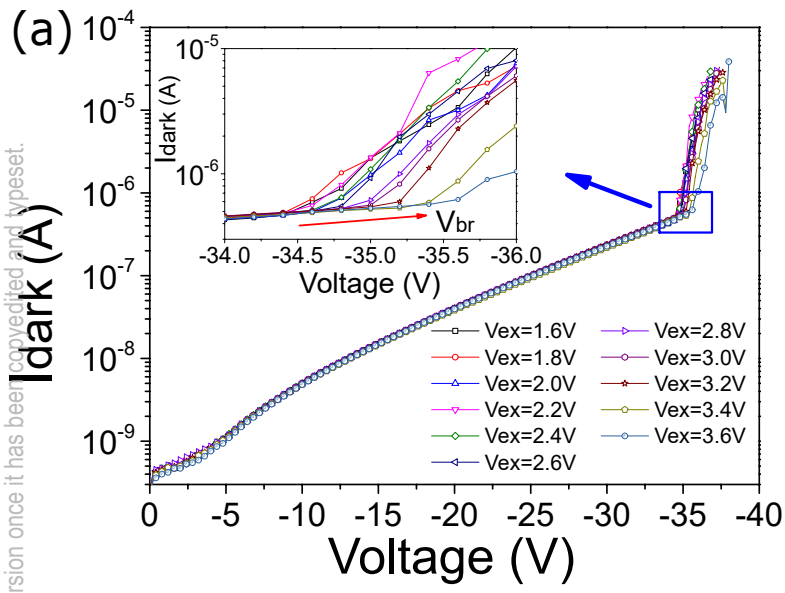
(b)

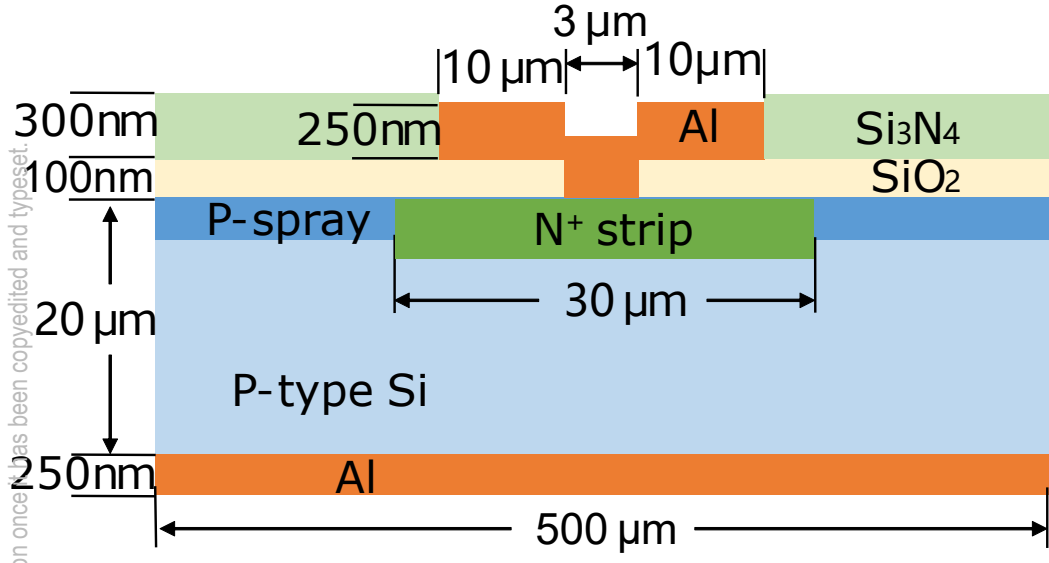


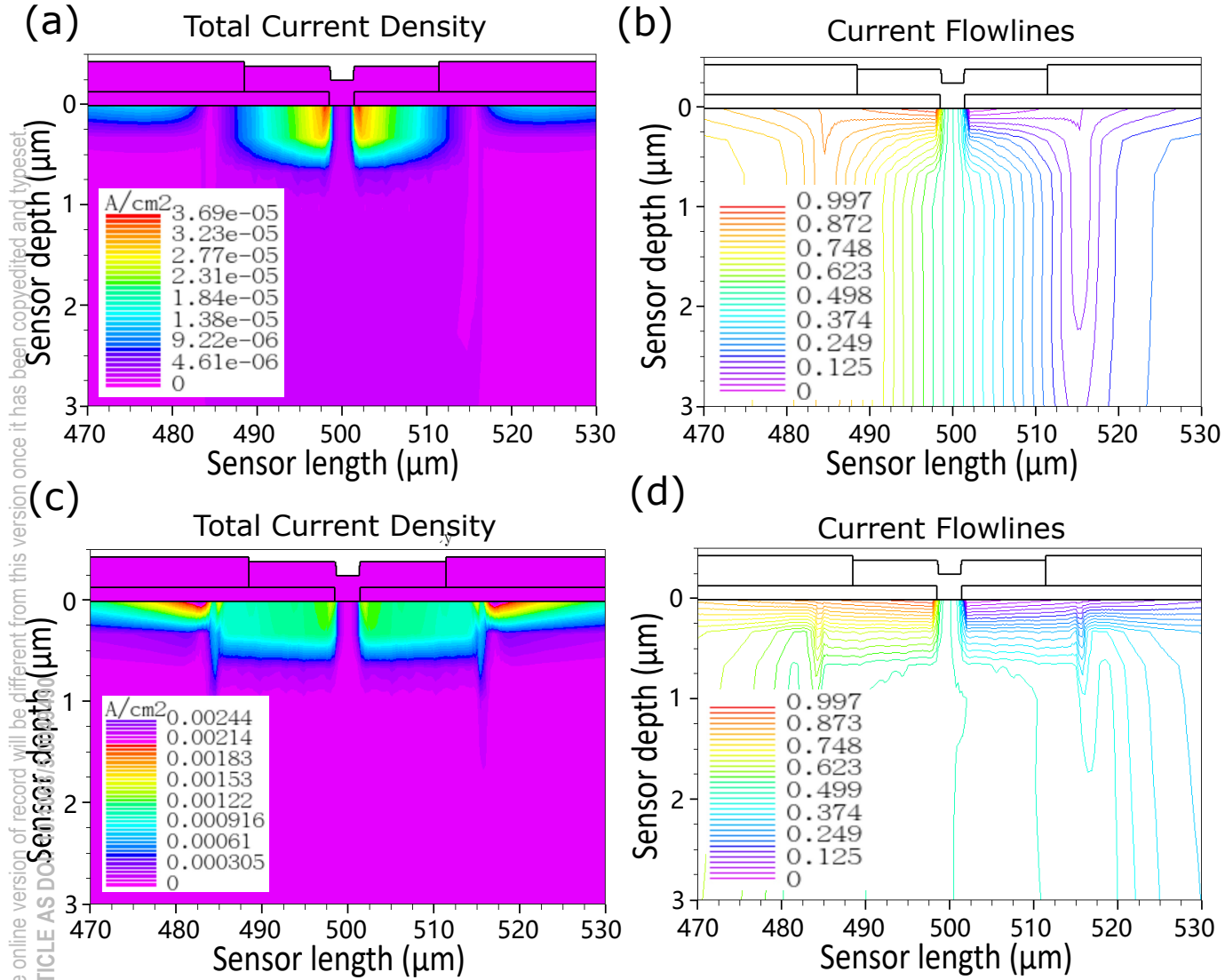


This is the author's peer reviewed, accepted manuscript. However, the online version of record will be different from this version once it has been copyedited and typeset.
PLEASE CITE THIS ARTICLE AS DOI: 10.1063/5.0049490

This is the author's peer reviewed, accepted manuscript. However, the online version of record will be different from this version once it has been copyedited and typeset.
PLEASE CITE THIS ARTICLE AS DOI: 10.1063/5.0049490

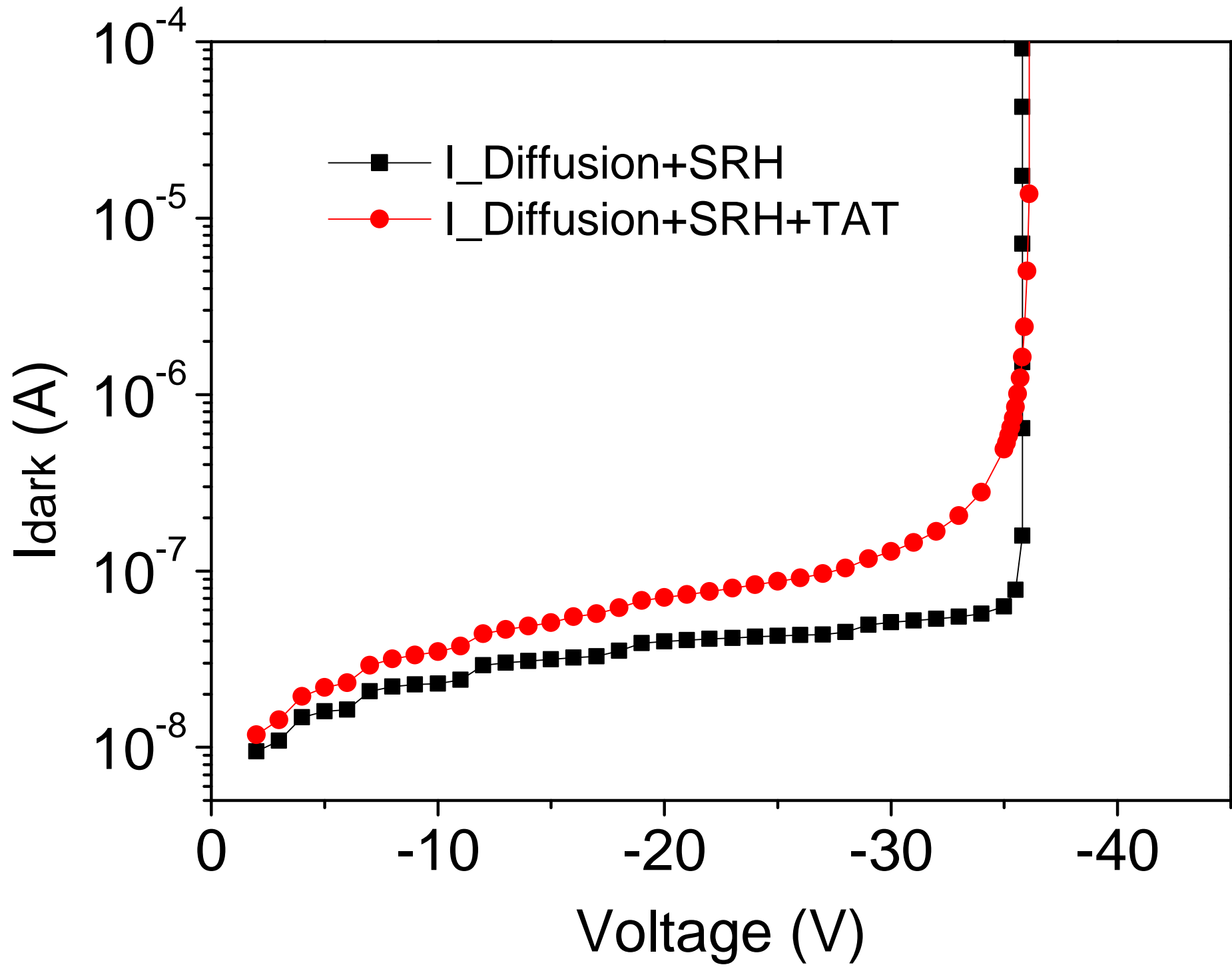




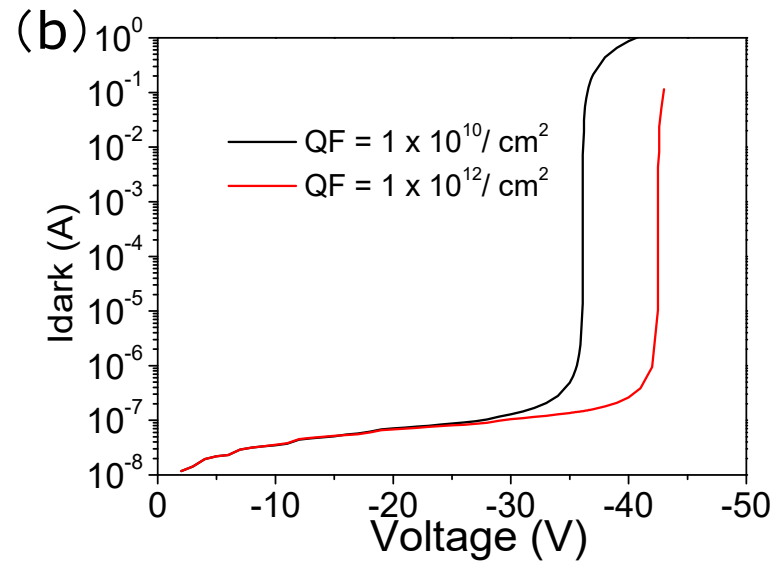
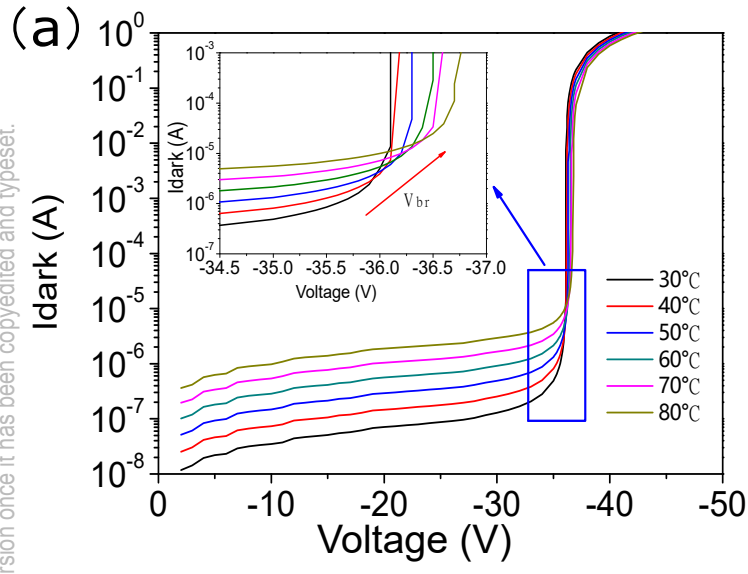


This is the author's peer reviewed, accepted manuscript. However, the online version of record will be different from this version once it has been copyedited and typeset. PLEASE CITE THIS ARTICLE AS DOI: 10.1063/1.5000000

This is the author's peer reviewed, accepted manuscript. However, the online version of record will be different from this version once it has been copyedited and typeset.
PLEASE CITE THIS ARTICLE AS DOI: 10.1063/5.0049490



This is the author's peer reviewed, accepted manuscript. However, the online version of record will be different from this version once it has been copyedited and typeset.
PLEASE CITE THIS ARTICLE AS DOI: 10.1063/5.0049490



This is the author's peer reviewed, accepted manuscript. However, the online version of record will be different from this version once it has been copyedited and typeset.
PLEASE CITE THIS ARTICLE AS DOI: 10.1063/5.0049490

